Maskless laser nano-lithography of glass through sequential activation of multi-threshold ablation

Cite as: Appl. Phys. Lett. **114**, 133107 (2019); https://doi.org/10.1063/1.5080344
Submitted: 07 November 2018 . Accepted: 20 March 2019 . Published Online: 05 April 2019

Yizhuo He, Jihua Zhang, Subhash Singh, Erik Garcell, Anatoliy Y. Vorobyev, Billy Lam, Zhibing Zhan, Jianjun Yang, and Chunlei Guo

Applied Physics Letters ARTICLE scitation.org/journal/apl

Maskless laser nano-lithography of glass through sequential activation of multi-threshold ablation

Cite as: Appl. Phys. Lett. **114**, 133107 (2019); doi: 10.1063/1.5080344
Submitted: 7 November 2018 · Accepted: 20 March 2019 ·
Published Online: 5 April 2019

Yizhuo He,[1,a)] Jihua Zhang,[1,a)] Subhash Singh,[1,2] Erik Garcell,[1] Anatoliy Y. Vorobyev,[1] Billy Lam,[1] Zhibing Zhan,[1] Jianjun Yang,[2] and Chunlei Guo[1,2,b)]

AFFILIATIONS

[1]The Institute of Optics, University of Rochester, Rochester, New York 14627, USA
[2]Changchun Institute of Optics, Fine Mechanics, and Physics, Changchun 130033, China

[a)]**Contributions:** Y. He and J. Zhang contributed equally to this work.
[b)]guo@optics.rochester.edu

ABSTRACT

Controllable nanofabrication is at the very foundation of nano-science and nano-technology. Today, ultrafast laser writing has been broadly adopted for micro-fabrication because of its ability to make precise and rapid processing of almost all types of materials in an ambient environment. However, direct laser writing is typically unsuitable for high-quality 2D nano-patterning. In this work, we introduce a maskless laser nano-lithographic technique that allows us to create regular 2D periodic nanopatterns on glass. Glass is a particularly challenging material since it does not absorb light readily. Our strategy starts with a glass sample being coated with a thin layer of metal, and then irradiated with a series of pulse bursts at progressively increasing fluence levels. This process allows us to sequentially activate a series of tailored physical processes that lead to the formation of regular 2D periodic nanopatterns on glass. The formation mechanism of this nano-patterning is also simulated numerically and further corroborated by a series of control experiments. We also show controllability in forming various shapes and sizes of nanopatterns through tailored fluence doses. Our technique provides a high-speed and low-cost method for glass nanofabrication.

Currently, common techniques used for nanofabrication include photolithography,[1] e-beam lithography,[2] focused ion beam,[3] nanoimprint lithography,[4] and colloidal lithography.[5] Recently, ultrafast laser processing[6] shows promises for nanofabrication with many advantages. First, laser processing is a simple and direct writing technique with the ability to process non-flat surfaces and almost all types of materials. Secondly, laser processing usually does not require masks or templates and can work under regular ambient conditions.[7] However, the major drawback of laser processing is that its resolution is usually limited by the light wavelength (on a micron scale) and sub-wavelength nanoscale structures produced by lasers usually lack high-quality and long-range regularity.[8,9] Although these irregular nanostructures have enabled a wide range of surface functionalities, such as the creation of black silicon and metals, superhydrophilic, superhydrophobic, and multifunctional surfaces,[6] the inherent nanoscale irregularities hinder the laser from being adopted as a viable tool for controllable nanofabrication.

Advancements were made in generating more regular sub-wavelength structures through laser processing. For example, periodic structures can be obtained on material surfaces over a large extended area by laser processing, which is referred to as laser induced periodic surface structures (LIPSSs).[6,10,11] A great amount of effort has been devoted to fabricating one-dimensional LIPSSs through laser ablation[9,12–15] and laser-assisted thermochemical methods.[16,17] Although these methods allow generation of high-quality one-dimensional LIPSSs, they cannot be readily used to generate two-dimensional (2D) LIPSSs by simply superimposing a second LIPSS array because the second step tends to smear out the first formed structures.[18] On the other hand, regular 2D surface nanostructures are far more difficult to produce but have more important applications, such as antireflection,[19] producing structural colors,[20] controlling light flow,[21] manipulating light polarizations,[22] biochemical sensing,[23] and data storage.[24] Recently, high-quality 2D periodic nanostructures have been produced on highly absorptive metals by us through time-delay laser pulses with cross polarizations.[25,26] However, ultrafast laser processing of dielectrics is far more challenging because of the low absorption from the transparent materials. Previous attempts on producing 2D LIPSSs on dielectrics have been reported by using circularly polarized lasers,[27]

double laser beams,[28] or template assisted methods,[29] but the resultant structures lack long-range uniformity and controllability in shape and size.[27–30] Apart from traditional nanolithography methods, template-free direct laser processing has never found success in producing controllable high-quality 2D nanopatterns in dielectric materials. Therefore, development of such a technique is strongly desired in the community. Especially, successful demonstration of high-quality periodic nanostructures on glass (or SiO_2), which is the most used dielectric material in daily lives, can find use in high-performance optics,[31] solar cells with enhanced efficiency,[32] eternal 5D data storage,[33] and low-loss metamaterials.[34]

In this work, we introduce a strategy for ultrafast laser processing in creating regular 2D periodic dielectric nanostructures on a glass surface. Our strategy starts with a glass sample coated with a thin layer of an Ag film. First, femtosecond (fs) laser pulses with relatively low fluences are used to irradiate the sample and break down the Ag film into Ag nanoparticles. Then, when irradiated with subsequent pulses with higher fluences, these Ag nanoparticles can induce enhanced local electric fields and assist creating glass nanostructures on the surface. Meanwhile, all the Ag nanoparticles are ablated away. Next, under several bursts of fs pulses, each with a specifically tailored fluence, these randomly distributed glass nanostructures grow larger and finally turn into hexagonal patterns through self-organization. We also demonstrate a degree of controllability in forming various shapes and sizes of nanopatterns with the total irradiation dose. In the past, different laser-matter interaction mechanisms were usually studied individually, with each mechanism playing a dominant role at a certain fluence level. Although many irradiation parameters can be varied in materials processing, such as laser polarization, pulse repetition rate, pulse numbers, and pulse temporal and spatial profiles, the fabrication of surface structures usually relies on the laser activating a dominant physical mechanism under a given condition. Controllable activation and stacking of a range of interaction mechanisms, at different fluence thresholds, has never been explored in the past for material processing. Our strategy essentially is to activate and combine a range of interaction mechanisms in a controllable sequence to produce high-quality nanofabrication using a laser beam alone.

The fabrication process of 2D periodic surface nanostructures is illustrated in Fig. 1. Glass coated with a 100-nm Ag film is exposed to a sequence of circularly polarized fs laser pulses (center wavelength: 790 nm, pulse duration: 62 fs, repetition rate: 1 kHz) at fluences increasing with time or pulse number. The laser beam was incident normally and focused by a lens (focal length $f = 250$ mm) onto the sample surface which is located ~2.5 mm after the focal plane. The laser ablation, including six fluence levels, starts at a low fluence of $F = 0.63$ J/cm^2 and sequentially increases to $F = 1.28$ J/cm^2, by steps of $\Delta F = 0.13$ J/cm^2. At each fluence, the sample was irradiated with $N = 2000$ laser pulses. The applied laser fluence was calculated by the measured laser power divided by the repetition rate and the spot area with a diameter about 170 μm, and was controlled by a half-wave plate and a linear polarizer. We analyze the surface morphology of Ag-film coated glass after laser treatment using a scanning electron microscope (SEM), whose images are shown in Fig. 2. Periodic nanostructure arrays are produced on the glass surface. According to energy-dispersive X-ray spectroscopy measurements, almost no Ag remains within the exposed area. Therefore, the Ag film is removed by fs laser ablation and periodic glass nanostructures are formed after exposure.

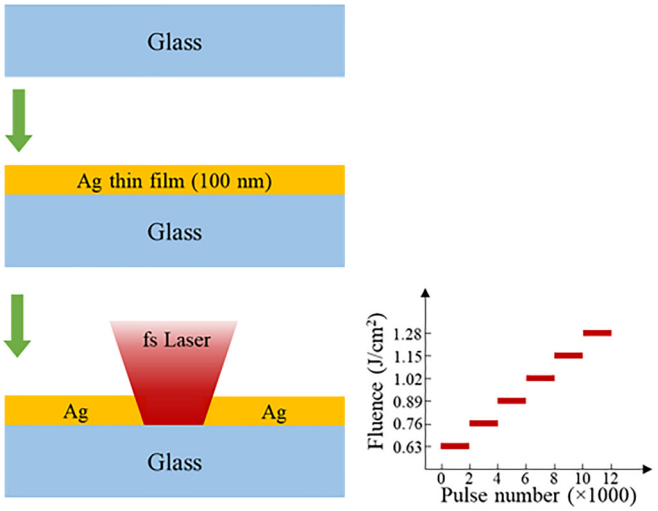

FIG. 1. Schematics of the fabrication process of periodic nanostructures on a glass surface. Glass slides were first coated with silver thin films by physical vapor deposition and were then processed by circularly polarized fs laser pulses. The laser fluence increases by $\Delta F = 0.13$ J/cm^2 every 2000 pulses.

Figures 2(a)–2(d) show four typical periodic nanostructures, Structure 1 (S1), Structure 2 (S2), Structure 3 (S3), and Structure 4 (S4), formed at different locations within the laser beam where the local laser fluences differ as $F_{S1} < F_{S2} < F_{S3} < F_{S4}$. The observation of different nanostructures S1, S2, S3, and S4 indicates that the obtained nanostructure morphology strongly depends on the total irradiation dose. The geometric parameters of these nanostructures are summarized in Table I. At a low irradiation dose, periodic nanostructures (S1) are formed with a size of about 630 nm in Fig. 2(a). The nanostructures are hexagonally arranged with a period of around 670 nm. The structure shape varies slightly for different individual nanostructures, including rhombus and rectangle shapes. As the irradiation dose increases, the nanostructures (S2) become more isotropic and turn into nanodomes with a diameter of about 530 nm in Fig. 2(b). At a higher irradiation dose, the nanodomes start to disappear and a regular array of nanoholes (S3) are formed with a diameter of 308 nm in Fig. 2(c). As shown in a zoom-in image in Fig. 2(e), the nanodomes do not disappear completely for S3. It should be noted that the small nanoparticles randomly distributed on the surface in Fig. 2(e) are Au-Pd nanoparticles that are deposited later for SEM observation. At even higher laser fluence, the nanodomes are completely removed in S4, resulting in an array of nanoholes with a diameter of 326 nm as shown in Figs. 2(d) and 2(f). Although the nanostructures S1–S4 differ in shape and size, they are all arranged hexagonally with almost identical structure periods of ~670 nm.

In order to gain three-dimensional information on the periodic nanostructures, the surface height distributions of S1, S2, S3, and S4 were measured with a UV laser scanning microscope. The height profiles are shown in Fig. 3. For S1, the height of the nanostructures is about 100 nm. Due to the small structure height, the periodic structure is hard to identify from the height profile. As the irradiation dose increases, the nanostructure height increases to about 200 nm for S2, and the distinct periodic nanodomes are observed in the height profile.

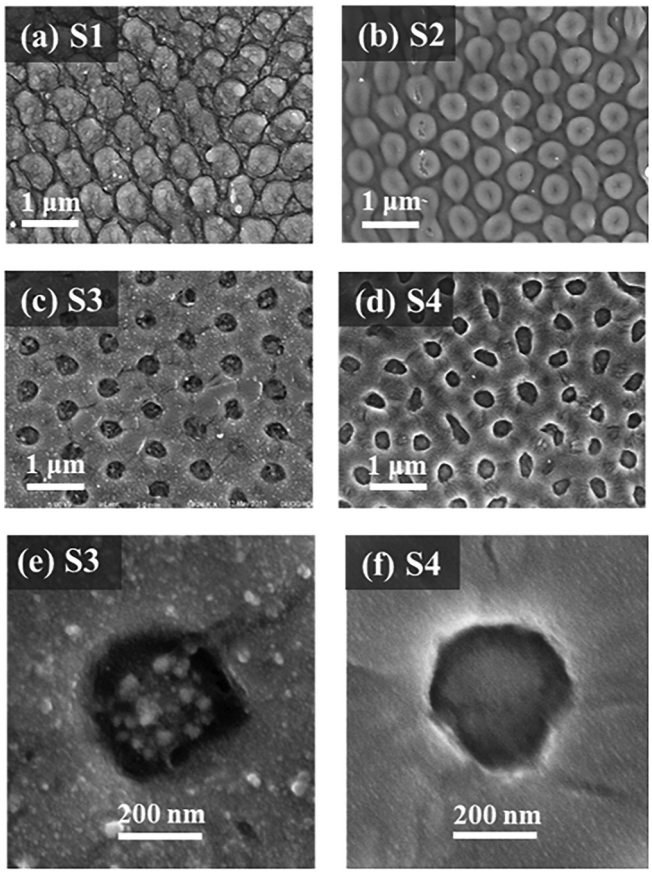

FIG. 2. SEM images of the glass surface nanostructures after ablation by a sequence of fs laser pulses at increasing fluences with pulse numbers. Different glass nanostructures (a) S1, (b) S2, (c) S3, and (d) S4 are produced for different local laser fluences $F_{S1} < F_{S2} < F_{S3} < F_{S4}$. (e) and (f) Zoom-in images of S3 and S4, respectively.

Obtained at a higher irradiation dose (S3), nanodomes are observed within nanoholes, represented in the height profile as peaks in the centers of valleys (nanoholes). The nanoholes have a depth of 200 nm and the nanodomes have a height of 400 nm (peak-to-valley difference). In S4, the central nanodomes are removed and only nanoholes are observed with a depth of 200 nm. The measured height profiles are consistent with the observation in SEM images in Fig. 2.

To understand the formation mechanisms of these ordered nanostructures, we performed a set of finite difference time domain simulations to study the structural formation dynamics. The electric fields near the nanostructures of S1, S2, and S3 were calculated under circular polarization illumination at a wavelength of 790 nm in order to find the location of the field enhancement where ablation will occur and to predict the structural change. Detailed geometric dimensions of S1, S2, and S3 and simulation results are given in supplementary material, Fig. S1. The calculated near field distributions successfully predict the structural change from S1 to S2, from S2 to S3, and from S3 to S4, when exposed to higher laser fluence.

TABLE I. Structural parameters of periodic nanostructures S1, S2, S3, and S4.

	S1	S2	S3	S4
Period (nm)	668 ± 36	651 ± 30	666 ± 41	681 ± 43
Size (nm)	630 ± 50	530 ± 15	308 ± 23	326 ± 35

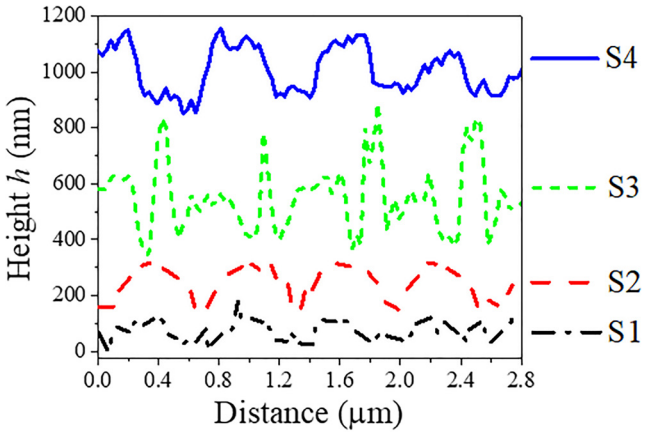

FIG. 3. Surface height profiles of the periodic nanostructures S1, S2, S3, and S4, as measured with a UV laser scanning microscope.

To further understand the dynamics of periodic ordering prior to the ordered nanostructures seen in Fig. 2, the sample surface was studied at different laser processing steps with laser fluences of 0.63 J/cm^2, 0.63 + 0.76 J/cm^2, 0.63 + 0.76 + 0.89 J/cm^2, 0.63 + 0.76 + 0.89 + 1.02 J/cm^2, 0.63 + 0.76 + 0.89 + 1.02 + 1.15 J/cm^2, and 0.63 + 0.76 + 0.89 + 1.02 + 1.15 + 1.28 J/cm^2. The SEM images in Figs. 4(a)–4(f) show the structure dynamics in forming S2 following laser irradiation. After the initial 2000 pulses at $F = 0.63$ J/cm^2, Ag micro-/nano-structures without regularity can be observed on the surface in Fig. 4(a), which are similar to those observed in a previous study created by fs laser ablation on the Ag film.[35] Exposed to another 2000 pulses at $F = 0.76$ J/cm^2, only Ag nanostructures are left in Fig. 4(b). A zoom-in image in the inset of Fig. 4(b) shows that Ag nanoparticles and nanoholes with diameters less than 80 nm exist on the glass surface. Note that in contrast to studies that rely on a regular pattern of particles that are first deposited by non-laser methods followed by laser processing,[36–38] our technique is a one-step process through laser only. After the next step (2000 pulses at $F = 0.89$ J/cm^2), Ag nanoparticles start to disappear and fine glass nanostructures with a size of about 100 nm are formed in some areas as shown in Fig. 4(c). After exposure to 2000 pulses at $F = 1.02$ J/cm^2, these nanostructures spread across the surface and grow larger as displayed in Fig. 4(d). After illuminated by 2000 pulses at $F = 1.15$ J/cm^2, the size of most nanostructures increases to about 500–550 nm. These nanostructures start to form regular hexagonal patterns as shown in Fig. 4(e). The hexagonal pattern is a stable configuration with low energy,[39,40] and therefore the hexagonal pattern is a natural result of self-organization (self-assembly) following our laser irradiation. Figure 4(f) shows the nanostructures after the final step of exposure to $F = 1.28$ J/cm^2 pulses, which are hexagonal nanodomes and are identical as those in Fig. 2(b). The particle areas in Figs. 4(c)–4(f) are analyzed with the statistical distributions shown in Figs. 4(g)–4(j), respectively. The particle area distribution clearly shows the evolution process of surface nanostructures.

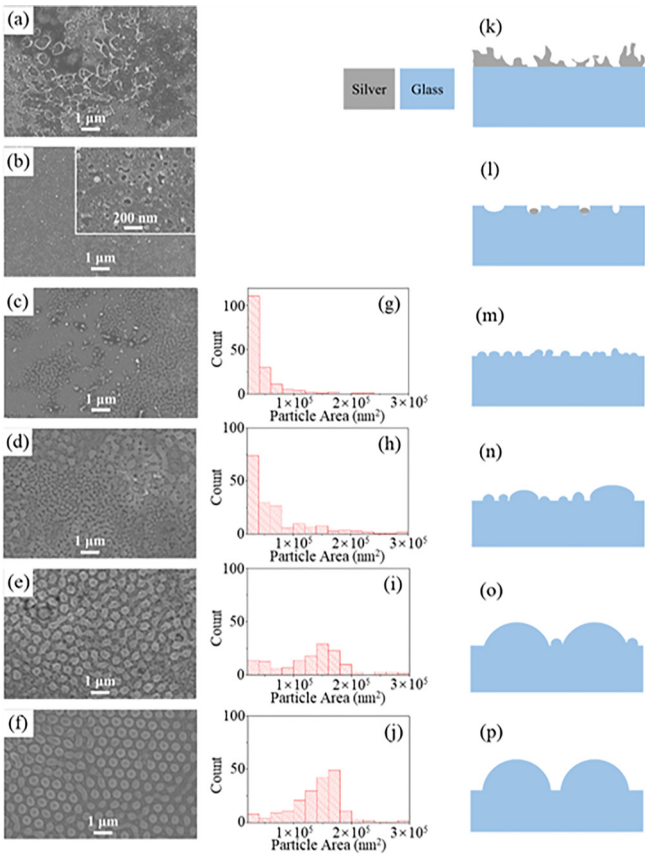

FIG. 4. SEM images of surface structures formed at different laser processing steps, under laser fluences of (a) 0.63 J/cm^2, (b) 0.63 + 0.76 J/cm^2, (c) 0.63 + 0.76 + 0.89 J/cm^2, (d) 0.63 + 0.76 + 0.89 + 1.02 J/cm^2, (e) 0.63 + 0.76 + 0.89 + 1.02 + 1.15 J/cm^2, and (f) 0.63 + 0.76 + 0.89 + 1.02 + 1.15 + 1.28 J/cm^2. At each fluence, the surface is exposed to 2000 pulses. (g)–(j) Distribution of the particle area of surface structures at steps (c)–(f). (k)–(p) Schematics of the surface structure evolution at steps corresponding to (a)–(f).

The area of nanostructures increases as more laser energy is deposited, and finally reaches a stable distribution centered at 1.8×10^5 nm^2, with a corresponding diameter of 480 nm, which is close to that (530 nm) by direct measurement in SEM images. The surface structure evolution process is summarized and shown in the schematics in Figs. 4(k)–4(p). The initial laser ablation breaks the Ag film into nanoparticles as illustrated in Figs. 4(k) and 4(l), which then induce localized laser ablation near Ag nanoparticles through the plasmonic enhanced electric near fields,[41,42] and assist creating nanostructures on glass. Ag nanoparticles start to be ablated away with increasing laser fluence in the next steps, and can no longer assist the laser ablation. Instead, multiphoton absorption and Coulomb explosion become the dominant ablation mechanisms at higher fluences.[43] The irregular nanostructures produced by Ag nanoparticle assisted ablation interact with the incident laser causing surface scattered waves, which interfere with the incident laser to induce 2D inhomogeneous laser energy deposition on the surface. The spatially modulated laser energy distribution leads to nonuniform laser ablation producing more and larger surface structures, which then further modulate the surface energy distribution by causing further surface scattered waves. Under such a feedback mechanism, the 2D surface structures develop into regular periodic nanostructures through self-organization with a period close to the incident laser wavelength as illustrated in Figs. 4(e) and 4(f).

Lastly, two verifying experiments were further performed to verify the roles of the metal film coating and the increasing laser fluence at each step. First, a soda-lime glass slide without any coatings was processed by fs laser pulses in the same sequence of fluences as shown in Fig. 1. The SEM images after each step show no periodic nanostructure formation (not shown here), which verify the indispensability of the metal coating in the fabrication. The most important contribution of the metal film to the formation of final glass structures is in creating initial fine nanostructures shown in Fig. 4(b) through plasmonic particle assisted laser ablation, which are crucial to the following self-organization process as discussed above. Second, Ag film coated glass was exposed to fs laser pulses at a fixed fluence during the ablation process. The experiments were performed at different fluences $F = 0.63$, 0.76, 0.89, 1.02, 1.15 and 1.28 J/cm^2 with pulse numbers N adjusted accordingly, so that the total irradiation doses are the same as the combined total dose of the sequence of increasing fluence. As a result, randomly distributed glass nanoparticles are produced on surfaces, indicating that dynamically increasing laser fluence is another key factor in producing periodic surface nanostructures. At the beginning of the laser processing, only the Ag film is ablated into micro-/nanoparticles, which requires a relatively low fluence due to the lower damage threshold of Ag than glass. The subsequent Ag nanoparticle assisted laser ablation producing glass nanostructures also requires relatively low fluence due to the already enhanced local electric fields. If a high laser fluence is applied at the beginning, Ag nanoparticles will be completely removed, leading to no nanostructure formation on glass and no subsequent self-organization. As discussed above, after Ag nanoparticles are ablated away, the ablation mechanism is switched to Coulomb explosion on glass. The higher damage threshold of glass requires an increased laser fluence to induce a self-organization process.

In conclusion, we develop a maskless laser nano-lithographic technique that allows us to create high-quality 2D periodic nanostructures on glass. By irradiating the sample with a series of pulse bursts at progressively increasing fluence levels, we sequentially activate a range of physical processes, including metal ablation, plasmonic assisted local ablation of dielectrics, and self-organization through Coulomb explosion and atomic surface diffusion, resulting in a regular pattern of 2D periodic nanostructures formed in a hexagonal pattern. By controlling the overall irradiation dose, we can obtain a pattern of different nanostructures, including nanobumps, nanodomes, and nanoholes. The formation mechanism of this nano-patterning process is further explained by FDTD simulations and additional experiments that corroborate our understanding. Although rich in physical mechanisms in nature, our processing technique is extremely simple to implement and enables the use of ultrafast lasers for nanofabrication at a scale smaller than their wavelength.

In future work, a large area of patterns can be fabricated by a scanning process using controlled beam profiles, in which the laser fluence at each location can change dynamically through scanning. It is also possible to improve the uniformity of the structures by using materials with higher electron-phonon coupling coefficients, as shown

in previous works.[44,45] Furthermore, controlling the critical dimension such as the period and the size of the nanopatterns can be realized by using different metal coatings or by using different irradiation wavelengths. However, these studies are beyond the scope of the current work and require further studies in future work.

See supplementary material for the finite difference time domain simulations of nanostructures S1, S2, and S3.

This work was supported by Bill & Melinda Gates Foundation, the U.S. Army Research Office, DARPA, and National Science Foundation.

REFERENCES

[1]B. J. Lin, C. R. Phys. **7**, 858 (2006).
[2]M. Altissimo, Biomicrofluidics **4**, 026503 (2010).
[3]C. S. Kim, S. H. Ahn, and D. Y. Jang, Vacuum **86**, 1014 (2012).
[4]L. J. Guo, Adv. Mater. **19**, 495 (2007).
[5]S. M. Yang, S. G. Jang, D. G. Choi, S. Kim, and H. K. Yu, Small **2**, 458 (2006).
[6]A. Y. Vorobyev and C. L. Guo, Laser Photonics Rev. **7**, 385 (2013).
[7]M. Malinauskas, A. Žukauskas, S. Hasegawa, Y. Hayasaki, V. Mizeikis, R. Buividas, and S. Juodkazis, Light Sci. Appl. **5**, e16133 (2016).
[8]A. Y. Vorobyev and C. L. Guo, Opt. Express **14**, 2164 (2006).
[9]A. Y. Vorobyev, V. S. Makin, and C. L. Guo, J. Appl. Phys. **101**, 034903 (2007).
[10]K. Sugioka, Nanophotonics **6**, 393 (2016).
[11]J. Bonse, J. Krüger, S. Höhm, and A. Rosenfeld, J. Laser Appl. **24**, 042006 (2012).
[12]J. C. Wang and C. L. Guo, J. Appl. Phys. **100**, 023511 (2006).
[13]A. Y. Vorobyev and C. L. Guo, J. Appl. Phys. **104**, 063523 (2008).
[14]M. Huang, F. L. Zhao, Y. Cheng, N. S. Xu, and Z. Z. Xu, ACS Nano **3**, 4062 (2009).
[15]M. V. Shugaev, I. Gnilitskyi, N. M. Bulgakova, and L. V. Zhigilei, Phys. Rev. B **96**, 205429 (2017).
[16]B. Öktem, I. Pavlov, S. Ilday, H. Kalaycıoğlu, A. Rybak, S. Yavaş, M. Erdoğan, and F. Ömer Ilday, Nat. Photonics **7**, 897 (2013).
[17]A. V. Dostovalov, V. P. Korolkov, V. S. Terentyev, K. A. Okotrub, F. N. Dultsev, and S. A. Babin, Quantum Electron. **47**, 631 (2017).
[18]Y. Ogata and C. L. Guo, Nano Rev. Exp. **8**, 1339545 (2017).
[19]P. Spinelli, M. A. Verschuuren, and A. Polman, Nat. Commun. **3**, 692 (2012).
[20]A. G. Dumanli and T. Savin, Chem. Soc. Rev. **45**, 6698 (2016).
[21]J. Valentine, S. Zhang, T. Zentgraf, E. Ulin-Avila, D. A. Genov, G. Bartal, and X. Zhang, Nature **455**, 376 (2008).
[22]M. Iwanaga, Sci. Technol. Adv. Mater. **13**, 053002 (2012).
[23]M. E. Stewart, C. R. Anderton, L. B. Thompson, J. Maria, S. K. Gray, J. A. Rogers, and R. G. Nuzzo, Chem. Rev. **108**, 494 (2008).
[24]H. H. Pham, I. Gourevich, J. K. Oh, J. E. N. Jonkman, and E. Kumacheva, Adv. Mater. **16**, 516 (2004).
[25]H. Z. Qiao, J. J. Yang, F. Wang, Y. Yang, and J. L. Sun, Opt. Express **23**, 26617 (2015).
[26]Q. Liu, N. Zhang, J. J. Yang, H. Z. Qiao, and C. L. Guo, Opt. Express **26**, 11718 (2018).
[27]O. Varlamova, F. Costache, J. Reif, and M. Bestehorn, Appl. Surf. Sci. **252**, 4702 (2006).
[28]M. Rohloff, S. K. Das, S. Hohm, R. Grunwald, A. Rosenfeld, J. Kruger, and J. Bonse, J. Appl. Phys. **110**, 014910 (2011).
[29]T. Sakai, N. Nedyalkov, and M. Obara, J. Phys. D **40**, 2102 (2007).
[30]J. Reif, O. Varlamova, S. Varlamov, and M. Bestehorn, Appl. Phys. A **104**, 969 (2011).
[31]Y. F. Li, J. H. Zhang, S. J. Zhu, H. P. Dong, F. Jia, Z. H. Wang, Z. Q. Sun, L. Zhang, Y. Li, H. B. Li, W. Q. Xu, and B. Yang, Adv. Mater. **21**, 4731 (2009).
[32]J. Zhu, C. M. Hsu, Z. F. Yu, S. H. Fan, and Y. Cui, Nano Lett. **10**, 1979 (2010).
[33]J. Zhang, A. Čerkauskaitė, R. Drevinskas, A. Patel, M. Beresna, and P. G. Kazansky, Proc. SPIE **9736**, 97360U (2016).
[34]S. Jahani and Z. Jacob, Nat. Nanotechnol. **11**, 23 (2016).
[35]Y. Dai, M. He, H. D. Bian, B. Lu, X. N. Yan, and G. H. Ma, Appl. Phys. A **106**, 567 (2012).
[36]Y. Zhou, M. H. Hong, J. Y. H. Fuh, L. Lu, B. S. Lukyanchuk, and Z. B. Wang, J. Alloys Compd. **449**, 246 (2008).
[37]K. Piglmayer, R. Denk, and D. Bäuerle, Appl. Phys. Lett. **80**, 4693 (2002).
[38]Y. Zhou, M. H. Hong, J. F. Ying-Hsi, L. Lu, S. T. Leng, and B. S. Lukyanchuk, Chin. Phys. Lett. **24**, 2947 (2007).
[39]G. M. Whitesides and B. Grzybowski, Science **295**, 2418 (2002).
[40]A. Katsuhiko, P. H. Jonathan, V. L. Michael, V. Ajayan, C. Richard, and A. Somobrata, Sci. Technol. Adv. Mater. **9**, 014109 (2008).
[41]D. Eversole, B. Luk'yanchuk, and A. Ben-Yakar, Appl. Phys. A **89**, 283 (2007).
[42]M. Terakawa and N. N. Nedyalkov, Adv. Opt. Technol. **5**, 17 (2016).
[43]I. Mirza, N. M. Bulgakova, J. Tomastik, V. Michalek, O. Haderka, L. Fekete, and T. Mocek, Sci. Rep. **6**, 39133 (2016).
[44]J. C. Wang and C. L. Guo, Appl. Phys. Lett. **87**, 251914 (2005).
[45]J. C. Wang and C. L. Guo, J. Appl. Phys. **102**, 053522 (2007).